Structure, Kinematics and Evolution of Elliptical Galaxies from Hydrodynamical Simulations

Ph.D. Dissertation by
José Oñorbe Bernis

advised by
Rosa Domínguez Tenreiro

Universidad Autónoma de Madrid
Dpto. Física Teórica

April 24, 2009

Outline

1. Introduction and Motivation

Outline

1. Introduction and Motivation
2. The Method: DEVA code

Outline

Outline

Elliptical Galaxies

Nearly-featureless oval forms with approximately elliptical isophotes

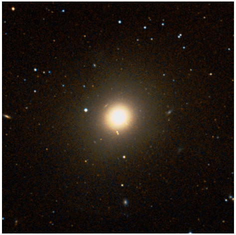

M89 (DSS2 data)

Elliptical Galaxies

Nearly-featureless oval forms with approximately elliptical isophotes

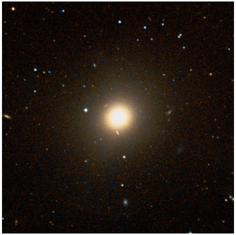

M89 (DSS2 data)

- Stellar scale: tight correlations among their structural and kinematical properties $\Rightarrow$ Homogeneus population

Elliptical Galaxies

Nearly-featureless oval forms with approximately elliptical isophotes

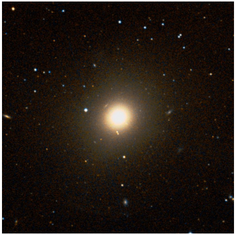

M89 (DSS2 data)

- Stellar scale: tight correlations among their structural and kinematical properties $\Rightarrow$ Homogeneus population
- However still very few is known about the mass and velocity distributions of the different elliptical mass components

Elliptical Galaxies

Nearly-featureless oval forms with approximately elliptical isophotes

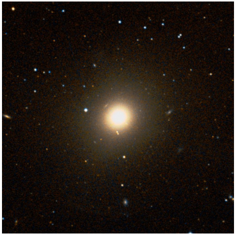

M89 (DSS2 data)

- Stellar scale: tight correlations among their structural and kinematical properties ⇒ Homogeneus population
- However still very few is known about the mass and velocity distributions of the different elliptical mass components
- How do they form?

How do they form?

Two main families of models based on the importance of two physical phenomena

- Monolithical Scenario: Gravitational collapse (Eggen et al. 1962, Larson 1974, Matteucci 2003)
- Hierarchical Scenario: Mergers (White & Rees 1978, Cole et al. 1994)

How do they form?

Two main families of models based on the importance of two physical phenomena

- Monolithical Scenario: Gravitational collapse (Eggen et al. 1962, Larson 1974, Matteucci 2003)
    - Passive-evolving stellar populations (downsizing) (Cadwell el al. 2003; Bernardi et al. 2003; Thomas et al. 2005; Jiménez el al. 2006; Noesk et al. 2007; Saracco et al. 2008; Daami et al. 2008)
    - Strong structural and kinematical relations (Djorgovski & Davis 1987; Dressler et al. 1987; Faber et al. 1987) and their lack of evolution (Treu & Koopmans 2004; Trujillo et al. 2004; McIntosh et al. 2005)
    - Population of massive, relaxed spheroids with old stellar populations already in place at high redshift (Cimatti et al. 2002, 2004; Stanford et al. 2004; Mobasher et al. 2005; Glazebrook 2005; Wiklind et al. 2008; Mobasher et al. 2009)
- Hierarchical Scenario: Mergers (White & Rees 1978, Cole et al. 1994)

How do they form?

Two main families of models based on the importance of two physical phenomena

- Monolithical Scenario: Gravitational collapse (Eggen et al. 1962, Larson 1974, Matteucci 2003)
- Hierarchical Scenario: Mergers (White & Rees 1978, Cole et al. 1994)
  - Signatures of merging observed by the moment out to intermediate zs (Le Fevre et al. 2000; Conselice et al. 2003; Cassata et al. 2005; Bell et al. 2005; Conselice 2008)
  - Growth of the total stellar mass bound up in bright red galaxies by a factor of about 2 since z=1 (Bell et al. 2004; Conselice et al. 2005: Faber et al. 2005; Conselice 2008)
  - Some star formation is still on at $z < 1.5$ (van Dokkum & Ellis 2003; van del Wel et al. 2004; Menateau et al. 2004; Kaviraj et al. 2008)
  - Increase of the E size at fixed stellar mass from $z = 1.5$ up to $z = 0$ (Trujillo et al. 2007; Saracco et al. 2008; Buitrago et al. 2008)

How do they form?

Two main families of models based on the importance of two physical phenomena

- Monolithical Scenario: Gravitational collapse (Eggen et al. 1962, Larson 1974, Matteucci 2003)
- Hierarchical Scenario: Mergers (White & Rees 1978, Cole et al. 1994)

Both processes DO OCCUR
which one of them, if any, is more important to explain stellar properties? mass assembly?

A Convenient Approach:

Study this problem in connection with the cosmological model

$\Longrightarrow$ Self-consistent hydrodynamical simulations

Outline

Self-Consistent Hydrodynamical Simulations

- Structure is generated by the growth of density fluctuations $\Leftarrow$ Good agreement between CMB and large-scale distribution of galaxies (> 100 Mpc) observations

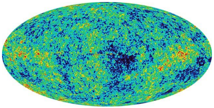

wmap sky map

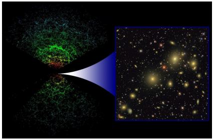

sdss galaxies

Self-Consistent Hydrodynamical Simulations

- Structure is generated by the growth of density fluctuations $\Leftarrow$ Good agreement between CMB and large-scale distribution of galaxies ($>$ 100 Mpc) observations
- Very solid theoretical framework for the formation of structures, but has still to be tested at lower scales

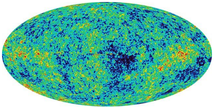

wmap sky map

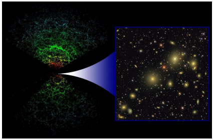

sdss galaxies

Self-Consistent Hydrodynamical Simulations

- Structure is generated by the growth of density fluctuations $\Leftarrow$ Good agreement between CMB and large-scale distribution of galaxies (> 100 Mpc) observations
- Very solid theoretical framework for the formation of structures, but has still to be tested at lower scales
- *Laboraty* experiments of astrophysics

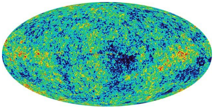

wmap sky map

$\Rightarrow$

LRZ-Munich Cluster

$\Rightarrow$

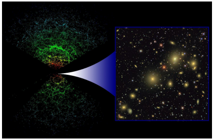

sdss galaxies

The DEVA Code (A. Serna, R. Domínguez-Tenreiro & A. Sáiz 2003)

- I.C.: homogeneously sampled perodic box with a montecarlo realization of the initial spectrum of density perturbations. (Model parameters based on WMAP3)
- Evolution or primordial inhomegeneities: AP3M (Gravity) + SPH (Hydrodynamic).
- Phenomenological parameterization of subresolution processes:
  - Star Formation: Kennicutt-Schmidt-law-like algorithm (ρ_{thres}, c_*) (Elmegrenn 2002)
  - Energy injection feedback (SN, AGN) is not explicitly included (Wada & Norman 2007, Scannapieco et al. 2008, Silk 2005)

The DEVA Code (A. Serna, R. Domínguez-Tenreiro & A. Sáiz 2003)

- I.C.: homogeneously sampled perodic box with a montecarlo realization of the initial spectrum of density perturbations. (Model parameters based on WMAP3)
- Evolution or primordial inhomegeneities: AP3M (Gravity) + SPH (Hydrodynamic).
- Phenomenological parameterization of subresolution processes:
  - Star Formation: Kennicutt-Schmidt-law-like algorithm (ρ_{thres}, c_*) (Elmegrenn 2002)
  - Energy injection feedback (SN, AGN) is not explicitly included (Wada & Norman 2007, Scannapieco et al. 2008, Silk 2005)

The DEVA Code (A. Serna, R. Domínguez-Tenreiro & A. Sáiz 2003)

- I.C.: homogeneously sampled perodic box with a montecarlo realization of the initial spectrum of density perturbations. (Model parameters based on WMAP3)
- Evolution or primordial inhomegeneities: AP3M (Gravity) + SPH (Hydrodynamic).
- Phenomenological parameterization of subresolution processes:
  - Star Formation: Kennicutt-Schmidt-law-like algorithm $(\rho_{thres},\ c_*)$ (Elmegrenn 2002)
  - Energy injection feedback (SN, AGN) is not explicitly included (Wada & Norman 2007, Scannapieco et al. 2008, Silk 2005)

The DEVA Code (A. Serna, R. Domínguez-Tenreiro & A. Sáiz 2003)

- I.C.: homogeneously sampled perodic box with a montecarlo realization of the initial spectrum of density perturbations. (Model parameters based on WMAP3)
- Evolution or primordial inhomegeneities: AP3M (Gravity) + SPH (Hydrodynamic).
- Phenomenological parameterization of subresolution processes:
  - Star Formation: Kennicutt-Schmidt-law-like algorithm $(\rho_{thres},\ c_*)$ (Elmegrenn 2002)
  - Energy injection feedback (SN, AGN) is not explicitly included (Wada & Norman 2007, Scannapieco et al. 2008, Silk 2005)

The DEVA Code (A. Serna, R. Domínguez-Tenreiro & A. Sáiz 2003)

- I.C.: homogeneously sampled perodic box with a montecarlo realization of the initial spectrum of density perturbations. (Model parameters based on WMAP3)
- Evolution or primordial inhomegeneities: AP3M (Gravity) + SPH (Hydrodynamic).
- Phenomenological parameterization of subresolution processes:
  - Star Formation: Kennicutt-Schmidt-law-like algorithm $(\rho_{thres}, \ c_*)$ (Elmegrenn 2002)
  - Energy injection feedback (SN, AGN) is not explicitly included (Wada & Norman 2007, Scannapieco et al. 2008, Silk 2005)

The DEVA Code (A. Serna, R. Domínguez-Tenreiro & A. Sáiz 2003)

- I.C.: homogeneously sampled perodic box with a montecarlo realization of the initial spectrum of density perturbations. (Model parameters based on WMAP3)
- Evolution or primordial inhomegeneities: AP3M (Gravity) + SPH (Hydrodynamic).
- Phenomenological parameterization of subresolution processes:
  - Star Formation: Kennicutt-Schmidt-law-like algorithm (ρ_{thres}, c_*) (Elmegrenn 2002)
  - Energy injection feedback (SN, AGN) is not explicitly included (Wada & Norman 2007, Scannapieco et al. 2008, Silk 2005)

$\Rrightarrow$ Galaxy-like objects naturally appear as a consequence of this evolution.

Elliptical Like Objects (ELOs). Building the Sample

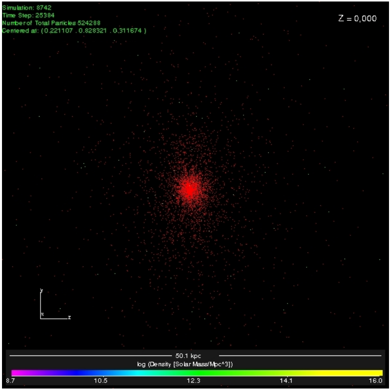

Figure: Orthogonal projection of the stellar and gas components of an ELO

- Visualization software and pipeline anylisis tool developed
- ELOs: dynamically relaxed stellar spheroids without extended discs
- Measure mass and velocity distributions at 3 different scales: Projected stellar scale (Observations), 3D Stellar scale ($\sim$ 20 kpc) and 3D Halo scale ($\sim$ 200 kpc)

Simulation Runs

- Several simulation runs to test: Star Formation algorithm, cosmological model, resolution (1.5, 0.5 kpc) and box size (10, 20, 80 Mpc)
- Also two versions of the code used: DEVA and P-DEVA

Sim.	Cosmo.	σ_8	ρ_{thres}	c_*	$N_{DM} + N_{bar}$	$L_{\rm box}$	ϵ
EA	WMAP3 (1)	1.18	6×10^{-25}	0.3	$64^3 + 64^3$	10	0.0015
EB	"	"	1.8×10^{-24}	**0.1**	"	"	"
EC	**WMAP3 (2)**	"	6×10^{-25}	0.3	"	"	"
ED	WMAP3 (1)	"	6×10^{-25}	0.3	$128^3 + 128^3$	10	**0.00075**
EF1	"	0.95	6×10^{-25}	0.3	$128^3 + 128^3$	**20**	0.0015
EF2	"	0.746	"	"	"	"	"
EF3	WMAP5	0.852	4.8×10^{-25}	"	esp.	**80**	"

- ELO samples were built for all these runs for several redshifts: $z = 0$, $z = 0.5$, $z = 1$ and $z = 1.5$

Outline

3D Halo Scale: Dark Matter Halos Profiles

Einasto Profile ($\equiv$ Navarro et al. 2004):

$$\rho^{\rm dark}(r) \propto \rho_{-2} \times exp[2\mu(r/r_{-2})^{1/\mu}]$$

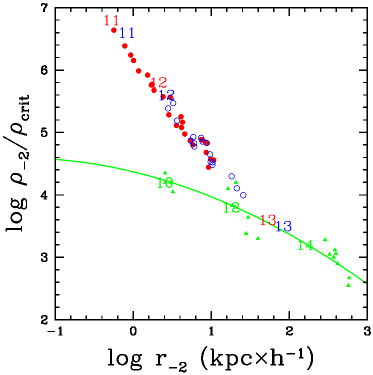

Figure: Characteristic radius and density (r_{-2}, ρ_{-2}) from fits to the Einasto profile for two samples of ELOs with different star formation parameters (EA and EB). Green points stand for results of pure N-body simulations (Navarro et al. 2004)

- Best fits by Einasto profile
- Universal profiles: two parameter family

  (Salvador-Solé et al. 2005, 2007)
- Adiabatic contraction. More important as virial mass decreases

  (Gnedin 2004)

2D Stellar Scale: Sérsic Profiles

$$I^{\rm light}(R) = I_0^{\rm light} exp[-b_n(R/R_e^{\rm light})^{1/n}] = \Sigma^{\rm star}(r)/\gamma^{\rm star}$$

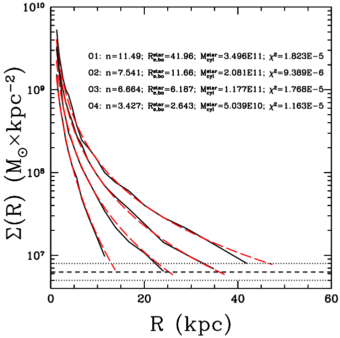

Figure: Projected stellar mass density profiles for different ELOs (black) along with their best fit Sérsic law (red)

- $\Sigma^{\rm star}(r)$ of ELOs can be fitted by a Sérsic law.
- Parameters show good agreement with observations

  (D'Onofrio 2001, Vazdekis et al. 2004)
- Projected stellar mass profiles present also universality properties

Dark Matter Fractions

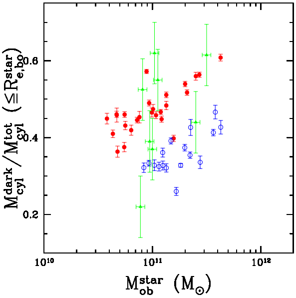

Figure: Dark matter fraction at the central regions (EA and EB samples). Green triangles stand for Cappellari et al. (2005) data

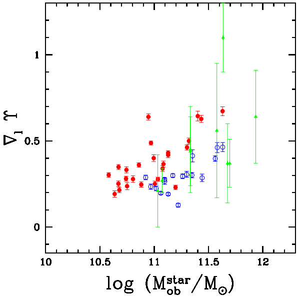

Figure: Gradients of the M^{dark}/M^{star} profiles (EA and EB samples). Green triangles stand for Napolitano et al. (2005) data

3D Total Mass Profiles

Introduction and Motivation
The Method: DEVA code
Results
Structural and Kinematical Properties at $z = 0$
Evolution of Fundamental Relations
A Scenario for Elliptical Formation
Conclusions

Power law: $r \sim \rho^{-\gamma}$

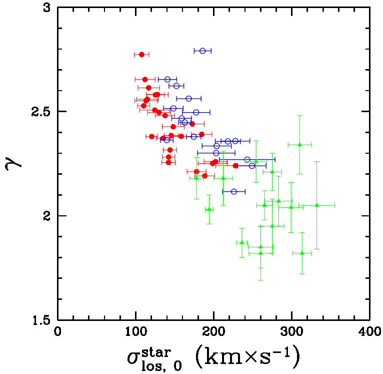

Figure: Logarithmic slopes to the total mass profiles (EA and EB samples). Green triangles stand for Koopmans et al. (2006) data

- Well fit by power-law well beyond effective radius
- Slope of the power-law increases with decreasing ELO mass

The Fundamental Plane and the Virial Theorem

Es show a large variety of correlations between photometric and kinematical parameters. The strongest one found up the moment is

The Fundamental Plane

$$\log R_{\rm e}^{\rm light} = a \times \log \sigma_0 + b \times \log < I^{\rm light} >_{\rm e} + c$$

$R_{\rm e}^{\rm light}$=projected light effective radius

$< I^{\rm light} >_{\rm e}$=mean surface brightness within the effective radius

σ_0=central velocity dispersion

Observational Relation

$a \simeq 1.5,\ b \simeq -0.77$

2D stellar scale

Virial Theorem Prediction

$a = 2,\ b = -1$

3D halo scale

total mass

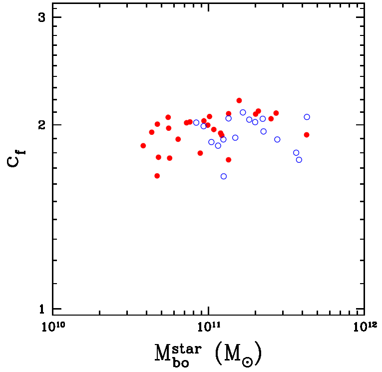

c_f form factors versus mass scale for EA and EB samples

- Virial Theorem predicts a strong correlation betweent total matter structure and kinematic parameters:
  $M_{\rm vir} = c_f \times (\sigma_{\rm 3,h}^{\rm tot})^2 \times r_{\rm e,h}^{\rm tot} / G$
- 3D Halo Scale: ELOs satisfy virial theorem

From Halo Scale to Stellar Scale

- 3D Halo scale parameters show tigh correlations with 3D Stellar scale ones
- Virial mass determines the ELO structure at kpc scales

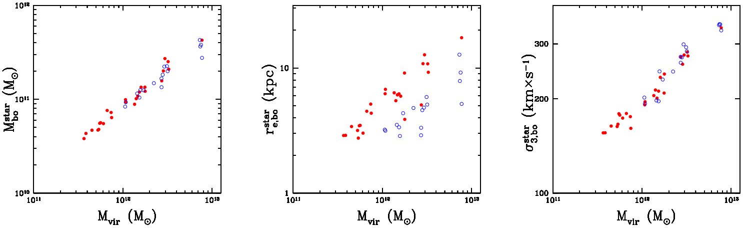

Virial mass ($M_{\rm vir}$) versus 3D stellar scale fundamental parameters ($r^{\rm star}_{\rm e,bo}$, $M^{\rm star}_{\rm bo}$, $\sigma^{\rm star}_{\rm 3,bo}$) for EA and EB samples

3D Stellar Scale: Intrynsic Dynamical Plane

- Fundamental parameters at these scale ($r^{\rm star}_{\rm e,bo}$, $M^{\rm star}_{\rm bo}$, $\sigma^{\rm star}_{\rm 3,bo}$) populate a flattened ellipsoid close to a two-dimensional plane: The IDP
- IDP is a consequence of the virial equilibrium

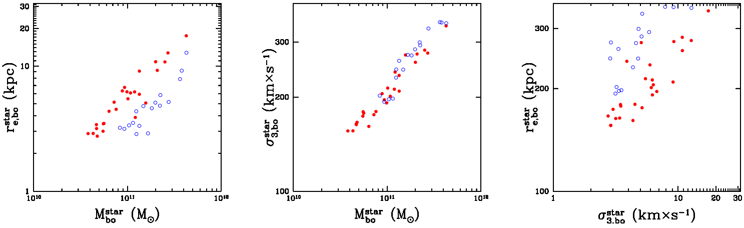

IDP projections for the EA and EB samples

The Fundamental Plane from our simulations

- Observational counterparts of our IDP: 2D quanties $R^{\rm star}_{\rm e,bo}$, $M^{\rm star}_{\rm cyl,bo}$, $\sigma^{\rm star}_{\rm los,0}$
- *Dynamical* space: mass not light-based parameters
- Changing space of coordinates to make things easy: $R^{\rm star}_{\rm e,bo}$, $M^{\rm star}_{\rm cyl,bo}$, $\sigma^{\rm star}_{\rm los,0}$ $\Rightarrow \kappa^D$ space which also uses mass, not light-based parameters Bender et al. (1992)

Relation between both spaces

$$\kappa_1^{\rm D} \equiv (2\log\sigma^{\rm star}_{\rm los,0} + \log R^{\rm star}_{\rm e,bo})/\sqrt{2},$$
$$\kappa_2^{\rm D} \equiv (2\log\sigma^{\rm star}_{\rm los,0} + 2\log\langle\Sigma^{\rm star}\rangle_e - \log R^{\rm star}_{\rm e,bo})/\sqrt{6},$$
$$\kappa_3^{\rm D} \equiv (2\log\sigma^{\rm star}_{\rm los,0} - \log\langle\Sigma^{\rm star}\rangle_e - \log R^{\rm star}_{\rm e,bo})/\sqrt{3}$$

Simple orthogonal coordinate transformation

The Fundamental Plane from our simulations

- Observational counterparts of our IDP: 2D quanties $R^{\rm star}_{\rm e,bo}$, $M^{\rm star}_{\rm cyl,bo}$, $\sigma^{\rm star}_{\rm los,0}$
- *Dynamical* space: mass not light-based parameters
- Changing space of coordinates to make things easy: $R^{\rm star}_{\rm e,bo}$, $M^{\rm star}_{\rm cyl,bo}$, $\sigma^{\rm star}_{\rm los,0} \Rightarrow \kappa^D$ space which also uses mass, not light-based parameters Bender et al. (1992)

Relation between both spaces

$$\kappa_1^{\rm D} \equiv (2 \log \sigma^{\rm star}_{\rm los,0} + \log R^{\rm star}_{\rm e,bo})/\sqrt{2},$$
$$\kappa_2^{\rm D} \equiv (2 \log \sigma^{\rm star}_{\rm los,0} + 2 \log \langle \sum^{\rm star} \rangle_e - \log R^{\rm star}_{\rm e,bo})/\sqrt{6},$$
$$\kappa_3^{\rm D} \equiv (2 \log \sigma^{\rm star}_{\rm los,0} - \log \langle \sum^{\rm star} \rangle_e - \log R^{\rm star}_{\rm e,bo})/\sqrt{3}$$

Simple orthogonal coordinate transformation

The Fundamental Plane from our simulations

- Observational counterparts of our IDP: 2D quanties $R^{\rm star}_{\rm e,bo}$, $M^{\rm star}_{\rm cyl,bo}$, $\sigma^{\rm star}_{\rm los,0}$
- *Dynamical* space: mass not light-based parameters
- Changing space of coordinates to make things easy: $R^{\rm star}_{\rm e,bo}$, $M^{\rm star}_{\rm cyl,bo}$, $\sigma^{\rm star}_{\rm los,0}$ $\Rightarrow \kappa^D$ space which also uses mass, not light-based parameters Bender et al. (1992)

Relation between both spaces

$$\kappa_1^{\rm D} \equiv (2\log\sigma^{\rm star}_{\rm los,0} + \log R^{\rm star}_{\rm e,bo})/\sqrt{2},$$
$$\kappa_2^{\rm D} \equiv (2\log\sigma^{\rm star}_{\rm los,0} + 2\log\langle\Sigma^{\rm star}\rangle_e - \log R^{\rm star}_{\rm e,bo})/\sqrt{6},$$
$$\kappa_3^{\rm D} \equiv (2\log\sigma^{\rm star}_{\rm los,0} - \log\langle\Sigma^{\rm star}\rangle_e - \log R^{\rm star}_{\rm e,bo})/\sqrt{3}$$

Simple orthogonal coordinate transformation

The Fundamental Plane from our simulations

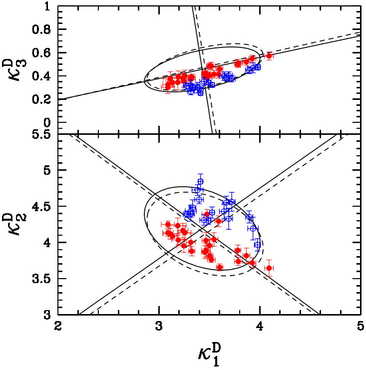

Figure: Edge-on projection (top panel) and nearly face-on projection (bottom panel) of the dynamical FP of ELOs in the κ^D variables for EA and EB samples). 2σ concentration ellipses for the SDSS early-type galaxy sample from Bernardi et al. (2003) in the z band (solid line) and the r band (dashed line).

The FP is the observational manifestation of the 3D IDP

The Tilt of the Fundamental Plane

ELOs at Halo scale satisfy the Virial Theorem & at the Projected Stellar scale show a good agreement with observed the Fundamental Plane relation $\Rightarrow$

The Origin of the Tilt?

$$L \propto c_{\rm vir}^{M} \times \frac{M_{\rm vir}}{M_*} \times \frac{M_*}{L}$$

- $L \propto \frac{M_*}{L}$ Change in the stellar content: Metallicity, age or IMF (Djorgovski 1988, Djorgovski et al. 1993, Renzini et al. 1993, Zepf & Silk 1996, Prugniel et al. 1996, Pahre et al. 1998, Mobasher et al. 1999, Bell et al. 2003, Kauffman et al. 2003)
- $L \propto \frac{M_{\rm vir}}{M_*}$ Variation of amount of dark-to-luminous matter. (Renzini et al. 1993, Ciotti et al. 1996, Pahre et al. 1998)
- $L \propto c_{\rm vir}^{M}$ Global structure of elliptical galaxies (Busarello et al.1997, Prugniel et al. 1997, Graham et al. 1997, Trujillo et al. 2004)

Origin of the Tilt

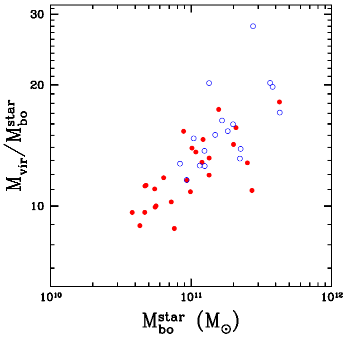

Figure: $M_{\rm vir}/M_{\rm bo}^{\rm star}$ ratios versus $M_{\rm bo}^{\rm star}$ for EA and EB samples

- Systematic trend with the mass scale in the relative content of the dark and baryonic mass components

Origin of the Tilt

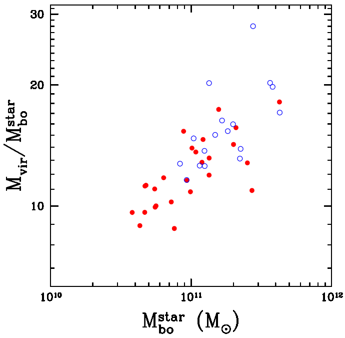

Figure: $M_{\rm vir}/M_{\rm bo}^{\rm star}$ ratios versus $M_{\rm bo}^{\rm star}$ for EA and EB samples

- Systematic trend with the mass scale in the relative content of the dark and baryonic mass components
- Origin: systematic decrease with increasing ELO mass, of the relative dissipation experienced by the baryonic mass component along ELO mass assembly

The Lack of Baryons

Figure: $f^{\rm bar}(r) = \rho^{\rm bar}(r)/\rho^{\rm tot}(r)$ profiles for EA and EB ELO samples

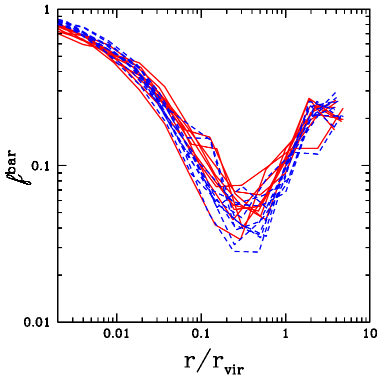

- ELOs are not baryonically closed up to $r_{\rm vir}$

The Lack of Baryons

Figure: $f^{\rm bar}(r) = \rho^{\rm bar}(r)/\rho^{\rm tot}(r)$ profiles for EA and EB ELO samples

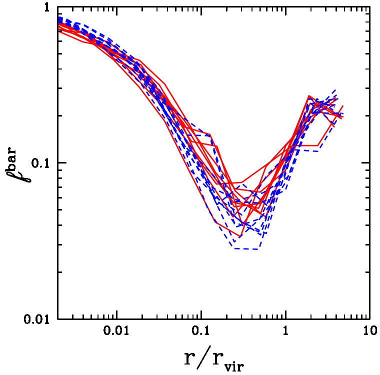

- ELOs are not baryonically closed up to $r_{\rm vir}$
- More massive ELOs miss baryons as compared with less massives ones, when we normalize to the dark matter content

The Lack of Baryons: Where are they?

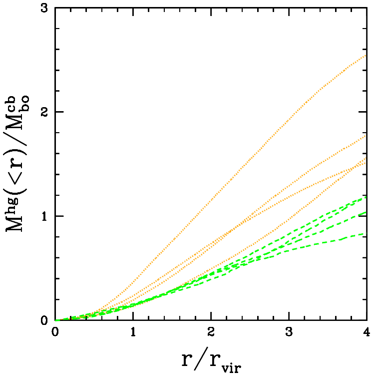

$M^{hg}(< r)/M^{cb}_{bo}$ profiles for isolated ELOs. ELOs with $1.5 \times 10^{12} \leq M_{vir} < 5 \times 10^{12} M_\odot$; ELOs with $M_{vir} < 1.5 \times 10^{12} M_\odot$

- Baryons that ELOs miss inside r_{vir} are found at the outskirts of the configuration as diffuse hot gas

The Lack of Baryons: Where are they?

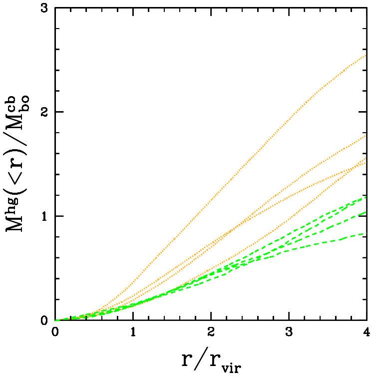

$M^{\rm hg}(< r)/M^{\rm cb}_{\rm bo}$ profiles for isolated ELOs. ELOs with $1.5 \times 10^{12} \leq M_{\rm vir} < 5 \times 10^{12} M_{\odot}$; ELOs with $M_{\rm vir} < 1.5 \times 10^{12} M_{\odot}$

- Baryons that ELOs miss inside $r_{\rm vir}$ are found at the outskirts of the configuration as diffuse hot gas
- This component is more important in more massive ELOs

Stellar Population Properties

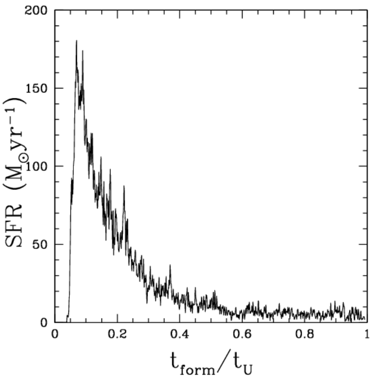

Figure: Star Formation Rate History (SFRH) of a typical ELO as obtained in the simulations (no modelling except SF probability implementation by K-S law)

- $\bar{t}$ = mean age of all stellar particles
- $\Delta t = t_{75} - t_{10}$ = width of the stellar population t_f = age at which the fraction f% of the stellar mass at $z = 0$ was already formed

Stellar Population Properties

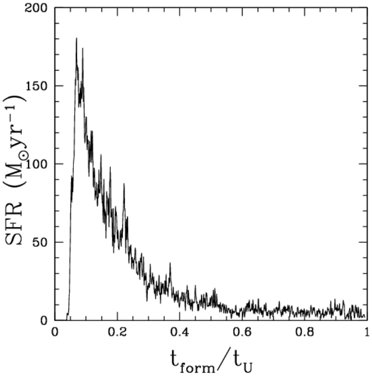

Figure: Star Formation Rate History (SFRH) of a typical ELO as obtained in the simulations (no modelling except SF probability implementation by K-S law)

- $\bar{t}$ = mean age of all stellar particles
- $\Delta t = t_{75} - t_{10}$ = width of the stellar population
  t_f = age at which the fraction $f\%$ of the stellar mass at $z = 0$ was already formed

Stellar Population Properties

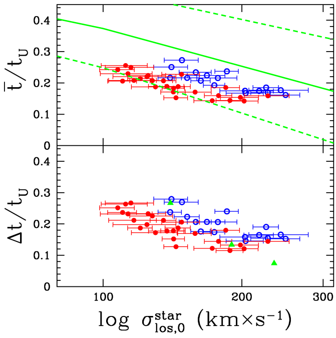

Upper Panel: Mean age of the stellar population.

Lower panel: The width of the stellar population age distribution. Observational data: Thomas et al. 2005. In both panels: EA and EB samples

- Stellar age properties show a clear trend with their structural and dynamical characteristical parameters
- Most stars have formed at high z on short timescales
- More massive objects have older means and narrower spreads in their stellar age distributions than less massive ones
- Same trends as those inferred from observations (downsizing)

Stellar Population Properties

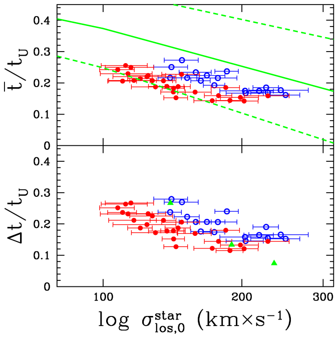

Upper Panel: Mean age of the stellar population. Lower panel: The width of the stellar population age distribution. Observational data: Thomas et al. 2005. In both panels: EA and EB samples

- Stellar age properties show a clear trend with their structural and dynamical characteristical parameters
- Most stars have formed at high z on short timescales
- More massive objects have older means and narrower spreads in their stellar age distributions than less massive ones
- Same trends as those inferred from observations (downsizing)

Stellar Population Properties

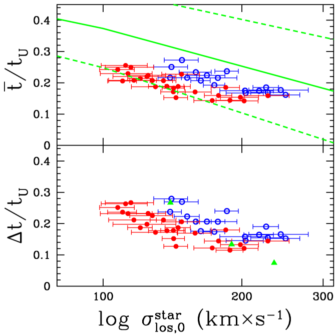

Upper Panel: Mean age of the stellar population.

Lower panel: The width of the stellar population age distribution. Observational data: Thomas et al. 2005. In both panels: EA and EB samples

- Stellar age properties show a clear trend with their structural and dynamical characteristical parameters
- Most stars have formed at high z on short timescales
- More massive objects have older means and narrower spreads in their stellar age distributions than less massive ones
- Same trends as those inferred from observations (downsizing)

Stellar Population Properties

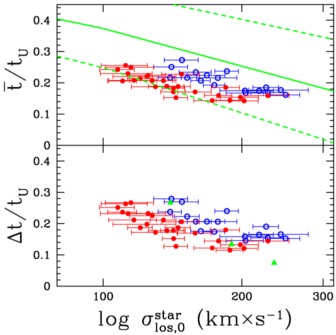

Upper Panel: Mean age of the stellar population.

Lower panel: The width of the stellar population age distribution. Observational data: Thomas et al. 2005. In both panels: EA and EB samples

- Stellar age properties show a clear trend with their structural and dynamical characteristical parameters
- Most stars have formed at high z on short timescales
- More massive objects have older means and narrower spreads in their stellar age distributions than less massive ones
- Same trends as those inferred from observations (downsizing)

Robustness of Results

Spherically averaged profiles (DM or baryons) of relaxed objects are independent of assembly paths (Salvador Solé et al. 2005, 2007). This results holds for changes in:

- box size

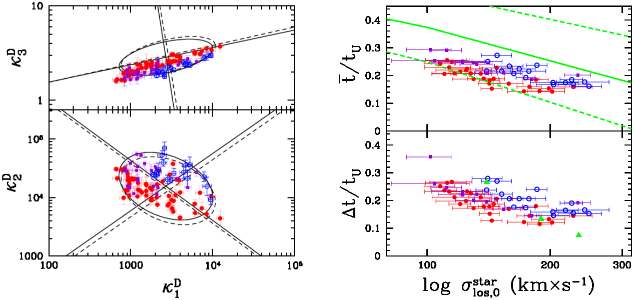

Left Panel: Fundamental Plane in kappa space. Right panel: Stellar population properties. In both panels: EA, EB and L_{box} = 80 Mpc sample (violet).

Robustness of Results

Spherically averaged profiles (DM or baryons) of relaxed objects are independent of assembly paths (Salvador Solé et al. 2005, 2007). This results holds for changes in:

- box size
- resolution
- cosmological parameters
- star formation parameters only change characteristic size
- code

Robustness of Results

Spherically averaged profiles (DM or baryons) of relaxed objects are independent of assembly paths (Salvador Solé et al. 2005, 2007). This results holds for changes in:

- box size
- resolution
- cosmological parameters
- star formation parameters only change characteristic size
- code

Box size and σ_8 parameters change the statistics of assembly paths $\Rightarrow$ clustering

Second Order Study: Rotational vs. Shape Diagram

- From spherical average profiles to 3D ellipsoids
- Study 2D and 3D shape and rotation descriptors

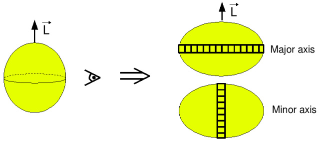

Upper panel: ELO ellipsoid approach and slit positions to mimic observational data

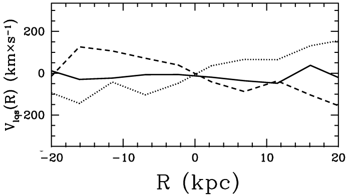

Lower panel: Full line: the major axis stellar LOS velocity profile along the spin direction for an ELO. Point and dashed lines: same as the continuous line taking the LOS direction normal to the ELO spin vector. This particular ELO rotates

- From spherical average profiles to 3D ellipsoids
- Study 2D and 3D shape and rotation descriptors

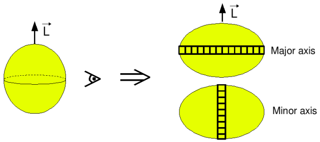

Upper panel: ELO ellipsoid approach and slit positions to mimic observational data

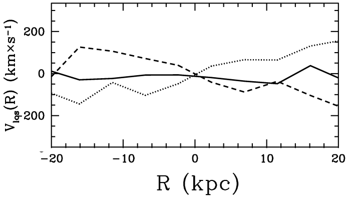

Lower panel: Full line: the major axis stellar LOS velocity profile along the spin direction for an ELO. Point and dashed lines: same as the continuous line taking the LOS direction normal to the ELO spin vector. This particular ELO rotates

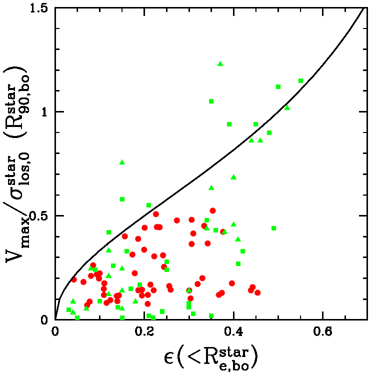

Figure: Projected shape parameter at $R^{\rm star}_{\rm e,bo}$ versus the projected rotational support parameter calculated at $R^{\rm star}_{\rm 90,bo}$ for the EA sample. Green triangles and squares stand for Cappellari et al. (2007) and Bender et al. (1994) data for ellipticals. Black solid line indicates the locus for oblate rotators (Binney, 1978).

- Shape and kinematic descriptors are closely related and in good agreement with observational data
- More massive ELOs show lower dispersion in rotational support and shape values

Second Order Study: Rotational vs. Shape Diagram

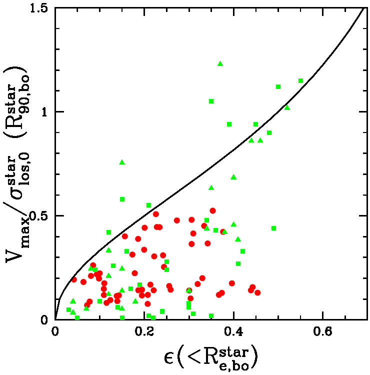

Figure: Projected shape parameter at $R^{\rm star}_{\rm e,bo}$ versus the projected rotational support parameter calculated at $R^{\rm star}_{\rm 90,bo}$ for the EA sample. Green triangles and squares stand for Cappellari et al. (2007) and Bender et al. (1994) data for ellipticals. Black solid line indicates the locus for oblate rotators (Binney, 1978).

- Shape and kinematic descriptors are closely related and in good agreement with observational data
- More massive ELOs show lower dispersion in rotational support and shape values

Outline

Evolution of the Fundamental Plane

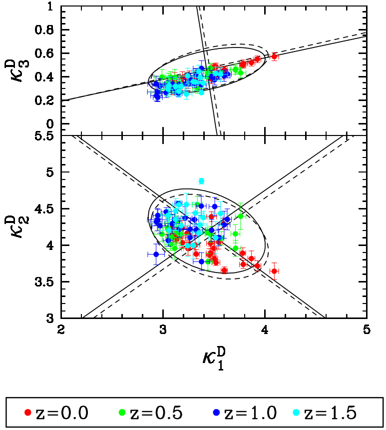

Figure: Edge-on projection (top panel) and nearly face-on projection (bottom panel) of the dynamical FP of ELOs in the κ^D variables for EA sample at different redshifts. Concentration ellipses stand as in previous figure.

- Fundamental Plane in dynamical space: κ^D
- Homogeneity of the relaxed ELO population up to $z = 1.5$ $\Rightarrow$ ELOs evolve along the Fundamental Plane (Treu & Koopmans 2004; Trujillo et al. 2004; McIntosh et al. 2005)
- κ_1^D vs κ_2^D evolution: lower dissipation per unit mass for mass assembly as we go to lower redshifts

Evolution of the Fundamental Plane

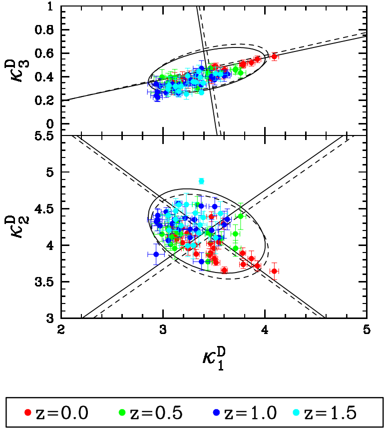

Figure: Edge-on projection (top panel) and nearly face-on projection (bottom panel) of the dynamical FP of ELOs in the κ^D variables for EA sample at different redshifts. Concentration ellipses stand as in previous figure.

- Fundamental Plane in dynamical space: κ^D
- Homogeneity of the relaxed ELO population up to $z = 1.5$ $\Rightarrow$ ELOs evolve along the Fundamental Plane (Treu & Koopmans 2004; Trujillo et al. 2004; McIntosh et al. 2005)
- κ_1^D vs κ_2^D evolution: lower dissipation per unit mass for mass assembly as we go to lower redshifts

Evolution of the Fundamental Plane

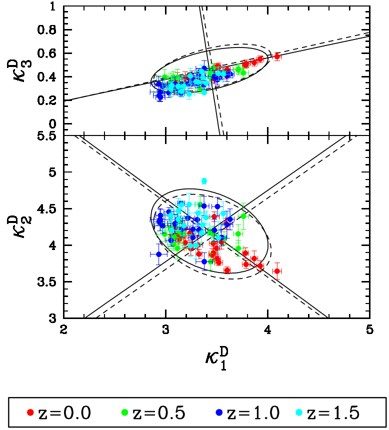

Figure: Edge-on projection (top panel) and nearly face-on projection (bottom panel) of the dynamical FP of ELOs in the κ^D variables for EA sample at different redshifts. Concentration ellipses stand as in previous figure.

- Fundamental Plane in dynamical space: κ^D
- Homogeneity of the relaxed ELO population up to $z = 1.5$ $\Rightarrow$ ELOs evolve along the Fundamental Plane (Treu & Koopmans 2004; Trujillo et al. 2004; McIntosh et al. 2005)
- κ_1^D vs κ_2^D evolution: lower dissipation per unit mass for mass assembly as we go to lower redshifts

Evolution of the Shape vs. Rotation Diagram

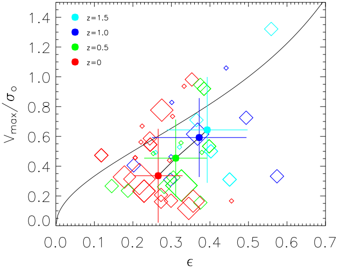

Figure: $V_{\rm max}/\sigma^{\rm star}_{\rm los,0}$ vs ϵ diagram for massive ($M^{\rm star}_{\rm bo} > 1 \times 10^{11} M_\odot$) ELOs of the EA sample at different z. Filled circles give a mean for each redshift. Size of the simbol gives the accumulated number of major mergers that a system has undergone. Black solid curve is the locus of the oblate rotators (Binney 1978).

- Evolution towards rounder objects with less rotational support, driven by dry merging
- Some exceptions if mergers involve a relative high amount of specific angular momentum

Evolution of the Shape vs. Rotation Diagram

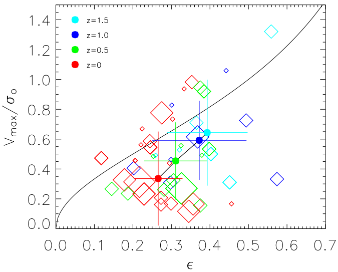

Figure: $V_{\max}/\sigma^{\rm star}_{\rm los,0}$ vs ϵ diagram for massive ($M^{\rm star}_{\rm bo} > 1 \times 10^{11} M_{\odot}$) ELOs of the EA sample at different z. Filled circles give a mean for each redshift. Size of the simbol gives the accumulated number of major mergers that a system has undergone. Black solid curve is the locus of the oblate rotators (Binney 1978).

- Evolution towards rounder objects with less rotational support, driven by dry merging
- Some exceptions if mergers involve a relative high amount of specific angular momentum

Outline

ELO Formation in Hydrodynamical Simulations

- When were stars formed?
- When was the ELO mass assembled?

ELO Formation in Hydrodynamical Simulations

- When were stars formed? $\Rightarrow$ SFRHs
- When was the ELO mass assembled?

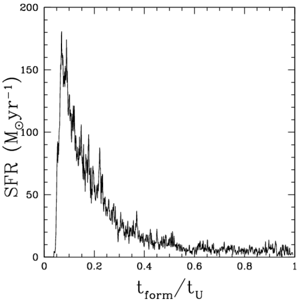

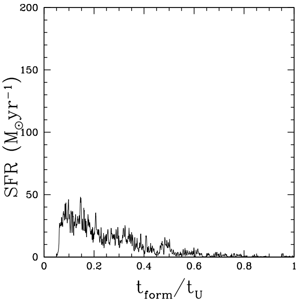

Star Formation Rate Histories of two typical ELOs versus the Universe age. M_{bo}^{star} (Right) $>$ M_{bo}^{star} (Left)

ELO Formation in Hydrodynamical Simulations

- When were stars formed? $\Rightarrow$ SFRHs
- When was the ELO mass assembled? $\Rightarrow$ MATs

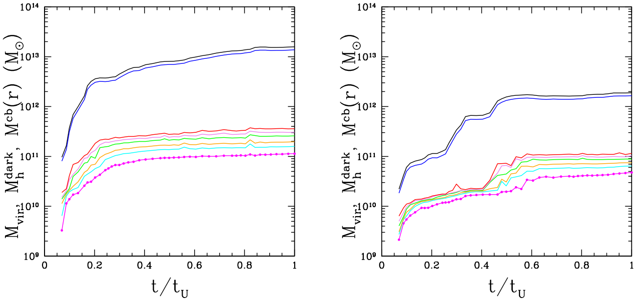

Mass Aggregation track along the main branches of the merger tree for two typical ELOs. $M_{\rm bo}^{\rm star}$ (Right) $>$ $M_{\rm bo}^{\rm star}$ (Left). Both panels give the total mass of the halo (black) and dark matter (blue) at $r_{\rm vir}$. Color lines stand for the baryonic mass of the ELO at different fixed radii (3, 6, 9, 15, 21, 30 kpc)

ELO Formation in Hydrodynamical Simulations

- When were stars formed? $\Rightarrow$ SFRHs
- When was the ELO mass assembled? $\Rightarrow$ MATs

Both analyses indicate that two different phases operate along ELO mass assembly

Two Phases Scenario

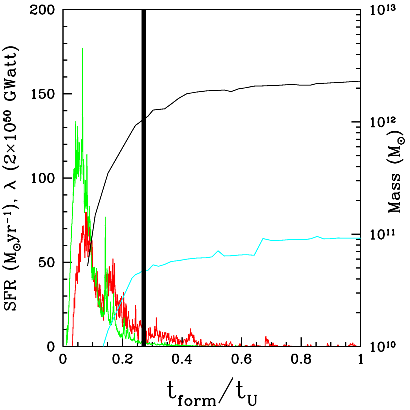

Figure: SFRH, Cooling rate history and Mass Aggregation Track for a massive ELO (black: virial mass; cyan: baryonic matter at 20 kpc). Black column indicates the separation

- Fast phase: multiclump collapse

  (Thomas et al. 1999)
- Slow phase: dry mergers

Two Phases Scenario

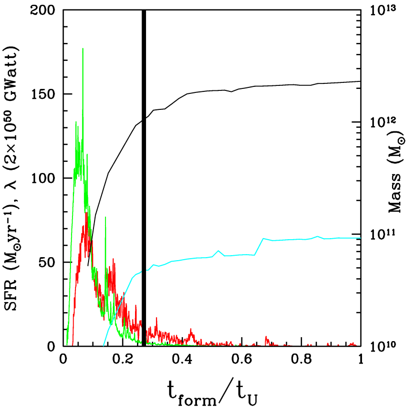

Figure: SFRH, Cooling rate history and Mass Aggregation Track for a massive ELO (black: virial mass; cyan: baryonic matter at 20 kpc). Black column indicates the separation

- Fast phase: multiclump collapse
  (Thomas et al. 1999)
  - High merger rate
  - Most of the dissipation occurs
  - Most of the stars are formed
  - Not much gas is left
  - Fundamental Plane settled down
- Slow phase: dry mergers

Two Phases Scenario

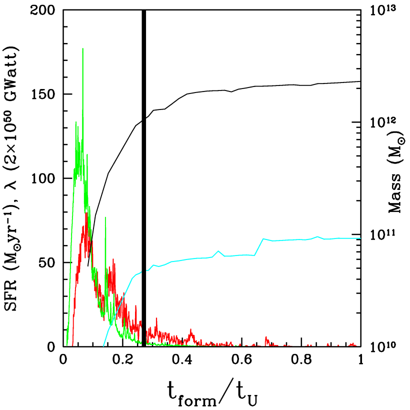

Figure: SFRH, Cooling rate history and Mass Aggregation Track for a massive ELO (black: virial mass; cyan: baryonic matter at 20 kpc). Black column indicates the separation

- Fast phase: multiclump collapse
  (Thomas et al. 1999)
- Slow phase: dry mergers
  - Low merger rate
  - ELOs grown by non-dissipative mergers and/or accretion
  - FP is conserved
  - Stellar formation rare although possible if is any gas left

Two Phases Scenario

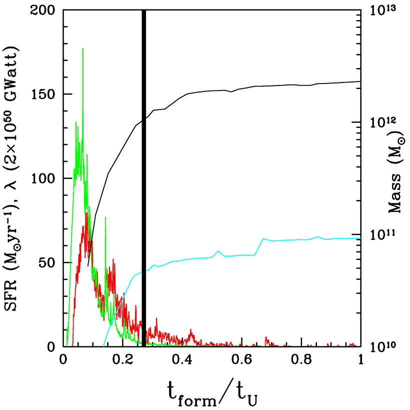

Figure: SFRH, Cooling rate history and Mass Aggregation Track for a massive ELO (black: virial mass; cyan: baryonic matter at 20 kpc). Black column indicates the separation

- Fast phase: multiclump collapse
  (Thomas et al. 1999)
- Slow phase: dry mergers

A formation scenario emerges where MERGERS play a very important role, but COLLAPSE - INDUCED processes are also very important at high z (De Lucia et al. 2006)

Accreting and Expelling Gas in ELOs

Figure: Baryon fraction, $f^{\rm bar} = M_{\rm h}^{\rm bar}/M_{\rm vir}$, at different redshifts for the EA samples

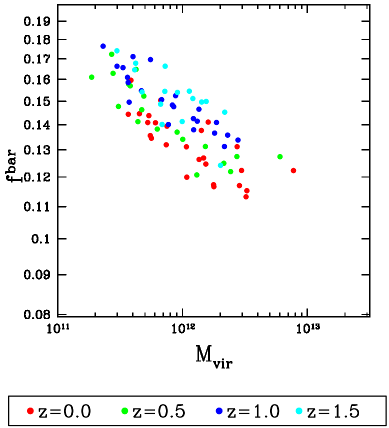

- $f^{\rm bar}$ lower than the average cosmic fraction (0.171) $\Rightarrow$ ELOs are not baryonically closed at any redshift
- The lack of baryons increase with mass at any redshift
- When and where are baryons heated?
- Where are they?

Accreting and Expelling Gas in ELOs

- Standard model: Gas falling into dark matter potential is shock-heated to the virial temperature and the slowly cools and travel inwards (White & Rees, 1978)
- High time resolution simulations $\Delta t = 6.9 \times 10^6 yr$
- Follow baryonic component that at $z = 0$ is forming the ELO

Accreting and Expelling Gas in ELOs

- Standard model: Gas falling into dark matter potential is shock-heated to the virial temperature and the slowly cools and travel inwards (White & Rees, 1978)
- High time resolution simulations $\Delta t = 6.9 \times 10^6 yr$
- Follow baryonic component that at $z = 0$ is forming the ELO

Accreting and Expelling Gas in ELOs

- Standard model: Gas falling into dark matter potential is shock-heated to the virial temperature and the slowly cools and travel inwards (White & Rees, 1978)
- High time resolution simulations $\Delta t = 6.9 \times 10^6 yr$
- Follow baryonic component that at $z = 0$ is forming the ELO

Accreting and Expelling Gas in ELOs

Figure: Histogram of the maximum temperature reached by all the baryonic particles inside $r_{\rm bo}$ of two ELOs. Left: $M_{\rm bo}^{\rm star} \sim 3 \times 10^{11} M_{\odot}$. Right: $M_{\rm bo}^{\rm star} \sim 5 \times 10^{10} M_{\odot}$.

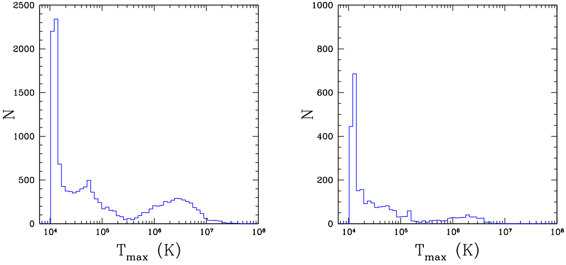

- Gas shows a bimodal history, two modes of gas accretion: Cold & Hot mode (Katz et al. 2003, Birnboim & Dekel 2003, Keres et al. 2008)

Accreting and Expelling Gas in ELOs

Figure: Histogram of the cooling time for all the baryonic particles inside $r_{\rm bo}$ that were accreted through the hot mode. Left: $M_{\rm bo}^{\rm star} \sim 3 \times 10^{11} M_{\odot}$. Right: $M_{\rm bo}^{\rm star} \sim 5 \times 10^{10} M_{\odot}$.

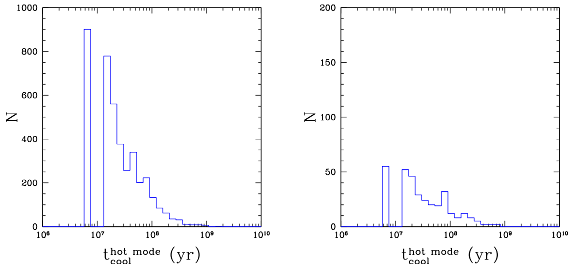

- Gas shows a bimodal history, two modes of gas accretion: Cold & Hot mode (Katz et al. 2003, Birnboim & Dekel 2003, Keres et al. 2008)
- Hot mode presents short cooling times and a strong link with the dynamical processes and ELO stellar mass

Accreting and Expelling Gas in ELOs

Figure: Star formation rate and the maximum temperature mass rate of the hot mode particles. Left: $M_{\rm bo}^{\rm star} \sim 3 \times 10^{11} M_{\odot}$. Right: $M_{\rm bo}^{\rm star} \sim 5 \times 10^{10} M_{\odot}$.

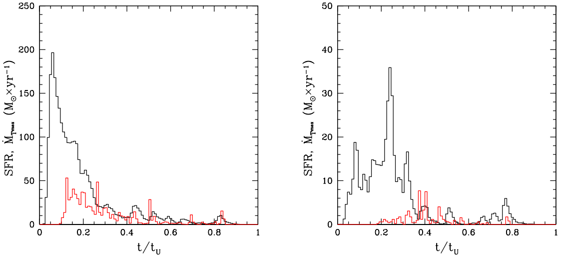

- Gas shows a bimodal history, two modes of gas accretion: Cold & Hot mode (Katz et al. 2003, Birnboim & Dekel 2003, Keres et al. 2008)
- Hot mode presents short cooling times and a strong link with the dynamical processes and ELO stellar mass

Accreting and Expelling Gas in ELOs

Figure: Baryonic mass accreted in cold mode over the total mass for ELOs of the 8716 simulation

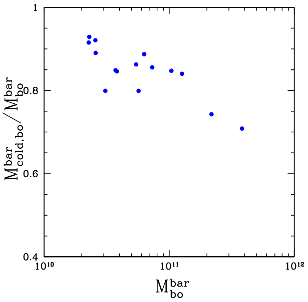

- More massive ELOs have more important hot accretion mode population
- Strong relation between the mass of the objects and the cold over hot mode fraction (Katz et al. 2003, Keres et al 2008)

Accreting and Expelling Gas in ELOs

Figure: Baryonic mass accreted in cold mode over the total mass for ELOs of the 8716 simulation

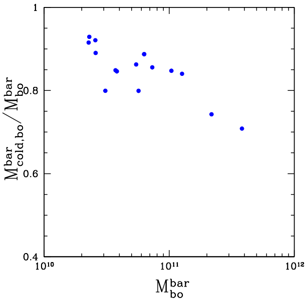

- More massive ELOs have more important hot accretion mode population
- Strong relation between the mass of the objects and the cold over hot mode fraction (Katz et al. 2003, Keres et al 2008)

Accreting and Expelling Gas in ELOs

Figure: Baryonic mass accreted in cold mode over the total mass for ELOs of the 8716 simulation

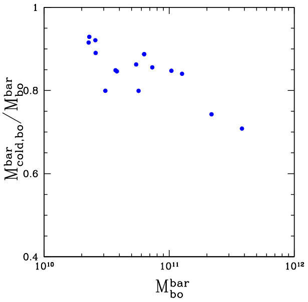

- More massive ELOs have more important hot accretion mode population
- Strong relation between the mass of the objects and the cold over hot mode fraction (Katz et al. 2003, Keres et al 2008)

Outline

Conclusions I

- **Structure and kinematical properties and age distributions of ELOS show a good agreement with observational data**

Conclusions I

- **Structure and kinematical properties and age distributions of ELOS show a good agreement with observational data**
- **ELOs are embedded in:**

Conclusions I

- **Structure and kinematical properties and age distributions of ELOS show a good agreement with observational data**
- **ELOs are embedded in:**
  - hot halos of diffuse gas that go beyond $r_{\rm vir}$

Conclusions I

- **Structure and kinematical properties and age distributions of ELOS show a good agreement with observational data**
- **ELOs are embedded in:**
  - hot halos of diffuse gas that go beyond r_{vir}
  - dark matter haloes that have experienced adiabatic contraction

Conclusions I

- **Structure and kinematical properties and age distributions of ELOS show a good agreement with observational data**
- **ELOs are embedded in:**
  - hot halos of diffuse gas that go beyond r_{vir}
  - dark matter haloes that have experienced adiabatic contraction
- **Spherically averaged profiles (DM or baryons) of relaxed objects are independent of assembly paths**

(Salvador Solé et al. 2005, 2007)

Conclusions II

- **ELOs are not baryonically closed systems up to $r_{\rm vir}$. This effect is increasing with ELO mass**

Conclusions II

- **ELOs are not baryonically closed systems up to $r_{\rm vir}$. This effect is increasing with ELO mass**
- **All these trends do not significantly depend on the star formation parameterization, cosmological model, box size or resolution**

Conclusions II

- **ELOs are not baryonically closed systems up to r_{vir}. This effect is increasing with ELO mass**
- **All these trends do not significantly depend on the star formation parameterization, cosmological model, box size or resolution**
- **Unified scenario where important current observations on E can be interrelated using a minimal set of hypothesis**: cosmological model (WMAP3 & WMAP5) and star formation (K-S law)

Outlook

- Metallicity evolution recently added by Martinez-Serrano et al. 2008 + Stellar Population Synthesis Models $\Rightarrow$ Direcly observable variables
- Recent large box size simulations open the door to calculate statistical properties to be compared with observations.
- Study of the rotational and shape descriptors recently introduced by 2D spectroscopy.

Evolution of Fundamental Relations: 3D

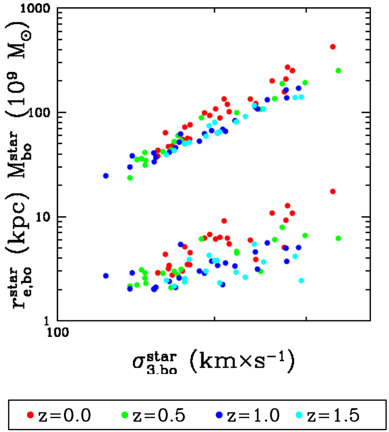

Figure: Evolution of the structural and kinematical fundamental parameters: $M_{\rm bo}^{\rm star}$, $r_{\rm e,bo}^{\rm star}$, $\sigma_{\rm 3,bo}^{\rm star}$ for EA runs at different redshifts.

- Some evolution of the most massive Es: decrease of the effective radius and increase of velocity dispersion for fixed mass
- Interpretation: different amount of dissipation that each ELO has suffered along its mass assembly